Full Paper

Propellants, Explosives, Pyrotechnics

DOI: 10.1002/prep.201800036

Preparation and Application of La_2O_3 and CuO Nano Particles as Catalysts for Ammonium Perchlorate Thermal Decomposition

Hossein Momenizadeh Pandas[a] and Mostafa Fazli*[a]

Abstract: Nanoparticles (NPs) from lanthanum oxide (La_2O_3) and copper oxide (CuO) with spherical morphology were synthesized through precursor calcinations of copper and lanthanum carbonate and then using a bioactive shell membrane of eggshell. X-ray diffraction (XRD) analysis and scanning electron microscopy (SEM) were used to evaluate particle size, chemical structure, purity and morphology of the synthesized La_2O_3 and CuO NPs. The XRD outcomes established the creation of the targeted compounds, SEM images obviously displayed morphology of the synthesized La_2O_3 and CuO as spherical NPs with average particle sizes of roughly 35 and 30 nm, correspondingly. The catalytic effects of these NPs on the thermal decomposition behavior of ammonium perchlorate (AP) were tested using differential scanning calorimetry (DSC) in coupling with thermogravimetric analysis (TG). The results of these experiments showed that the addition of 5% La_2O_3 nanoparticles has an attractive catalytic effect on the thermal decomposition of the AP. Moreover, AP thermal decomposition was facilitated by the addition of 5% CuO NPs. A more accurate comparison was made between the catalytic effects of synthesized NPs via computing their thermal decomposition activation energies (E), $\Delta S^{\#}$, $\Delta H^{\#}$ and $\Delta G^{\#}$ using diverse non-isothermal approaches.

Keywords: Lanthanum oxide · Copper oxide · Ammonium perchlorate (AP) · Nanocatalyst effect · Thermal decomposition kinetic · Thermodynamic parameters

1 Introduction

The unique properties of nanoparticles (NPS) have led researchers to focus on them in various fields, likewise catalysts, medicine, cosmetics, photonics, petroleum, and electronics [1–5]. Fabrication of various nanomaterials with specific particle size, certain morphology and high quality plays a key role in development of novel materials in different disciplines [6,7].

The more attention that is currently focused on earth oxides, both the realization of some of its unique catalytic properties and their availability in high purity, are enough to assess fundamental research [8].

NPs of lanthanum oxide (La_2O_3) are used as catalysts, optical devices, gas-exhaust convectors, etc. [9,10]. Also NPs of copper oxide (CuO) are applied as catalysts, in gas sensors, solar energy, electrical batteries, etc. [11–14]. Ammonium perchlorate or AP contains ammonium cation (NH_4^+) and perchlorate anion (ClO_4^-). The high oxygen content and the proper thermal stability of this inorganic salt are accountable for its extensive application as an interesting oxidant in solid propellants of rockets and pyrotechnic formulations [15–17]. By addition of metal oxides to AP as a burning rate modifier, its burning rate is effectually modified [18–21]. The high specific surface area of NPs from metal oxides such as La_2O_3 and CuO increase their properties at the burning rate modification of AP containing composite propellants. It has been reported that by adding small amounts of some metal oxides as nanocatalysts to AP, the performance and combustion behavior of AP containing composite solid propellants will be modified effectively [22].

Up to now, various reports have been published about the preparation of La_2O_3 and CuO NPs by diverse chemical approaches such as sol-gel, thermal solvolysis, hydrothermal methods, spray pyrolysis, reverse micellar, electro deposition etc. [23–25]. All of the approaches have some benefits, whereas some serious problems (such as presence of impurity in the final product, low safety, overwhelming and high cost) limit their widespread use [26]. Controlled precipitation approaches for instance membrane-aided routes make controlling the rate of crystal growth and therefore preparation of the product particles with definite particle size and particle size distribution [27]. In this study $La_2(CO_3)_3$ and $CuCO_3$ nano particles, the precursors of their metal oxides were fabricated by eggshell aided precipitation as proposed in the literature [28]. Thereafter, uniform and highly pure La_2O_3 and CuO nano particles were fabricated by ther-

[a] *H. M. Pandas, M. Fazli*
Chemistry Department, Faculty of Science, Semnan University, Semnan, 35195-363, Iran
Phone: +98 23 31533177
Fax: +98 23 33654110
**e-mail: mfazli@semnan.ac.ir*

mal calcination of their carbonate precursors. The main aims of this study were:

i) Preparation of highly pure $La_2(CO_3)_3$ and $CuCO_3$ nano particles via eggshell aided precipitation reaction.
ii) Fabrication of La_2O_3 and CuO nano particles as highly pure and uniform nano-catalysts for modifying thermal decomposition of AP.
iii) Assessing the effect of La_2O_3 and CuO nano particles for burning rate modification on AP thermal decomposition via thermal analysis methods, i.e., thermo-gravimetric analysis/differential scanning calorimetric analysis (TG-DSC).

Moreover, the thermo kinetics of thermal decomposition for the modified AP samples (with La_2O_3 and CuO nano-catalysts) were explored by the use of DSC data. Literature review showed that La_2O_3 have been used as a catalyst to characterize its effect on thermal decomposition of AP [29], while there are a few reports about the effect of CuO NPs prepared by ball milling route on the thermal behavior of AP [30].

2 Experimental

2.1 Materials

Laboratory grade NH_4ClO_4 powder (with medium particle size of about 80–100 μm) reagent grade sodium carbonate, lanthanum nitrate, and copper nitrate were purchased from Merck and used as received. Methyl isobutyl ketone (purity of MIBK > 99 %) was also acquired from Merck. Double distilled and deionized water was used for sample preparations.

2.2 Instrumentation

Synthesized La_2O_3 and CuO NPs were analyzed by scanning electron microscope (SEM model KYKY-EM3200, China). X-ray diffraction (XRD) and inductively coupled plasma (ICP) were used to characterize the chemical structure, morphology and size of particles. Before loading the samples on the instrument and recording SEM images, the AP samples were loaded on golden films. The films were prepared by a sputter coater (model SCD005, BAL-TEC, Switzerland). A Rigaku D/max 2500 V diffractometer equipped with graphite as monochromator and Cu target was applied to analyze the samples by the XRD. TG and DSC systems were used to explore the thermal behavior of the prepared nano-composites. DSC and TG analyses were carried out, respectively, on a DSC (Mettler Toledo Co., Switzerland) and a Mettler TA4000 thermal analyzer. The DSC tests were performed under the following operating conditions: mass of sample: about 3 mg; purging gas: N_2 at a flow rate of 50 mL min^{-1}; sample holder: alumina crucible; temperature range: 30 to 850 °C; applied heating rates: 5, 10, 15 and 20 °C min^{-1}. In the meantime, TG tests were achieved at the following operation conditions: mass of sample: about 3 mg; Sample holder: an alumina crucible; purging gas: N_2 at the flowing rate of 60 mL min^{-1}; applied heating rate: 10 °C min^{-1}; temperature range 50 to 800 °C.

2.3 Synthesis of $La_2(CO_3)_3$ and $CuCO_3$ Nanoparticles as Precursors

Copper carbonate and lanthanium carbonate nano particles were prepared from their nitrate salts and sodium carbonate by controlled precipitation using eggshell membrane as proposed previously [31]. Aimed at controlled ion transport during the precipitation reaction, the eggshell membrane was used as a bioactive membrane. This membrane could be prepared by removal of the outer shell of fresh eggshell. The occasioned membrane must be washed several times with deionized water. In order to produce the targeted carbonates, the reactor flask was divided into two sections via the eggshell membrane. Into one section 10 mL solution of 1.0 mol L^{-1} Na_2CO_3 was added and into the other section 10 mL solution of 1.0 mol L^{-1} either $La_2(NO_3)_3$ or $Cu(NO_3)_2$. Then, the reactor was kept at room temperature for rouphly 6 hours in order to get the targeted carbonate particles which form the sediment in the reactor bottom. Then, the produced carbonate particles precipitated at the bottom of the reactor, were separated (by 3 min centrifugation at 5000 RPM) and washed several times with distilled water. Finally the resulted product was washed with ethanol and dried at 80 °C for about 120 min.

2.4 Preparation of Lanthanum Oxide and Copper Oxide Nano Particles by Calcination of Their Precursors

Lanthanum oxide and copper oxide NPs were prepared by calcination of the carbonate precursors. La_2 $(CO_3)_3$and $CuCO_3$ nano particles acquired in the earlier stage were employed for calcinations. The precursors were thermally decomposed at 650 °C in the furnace under static air atmosphere for 3 hours. About 2 g of the carbonate precursor were loaded in an alumina container (with dimensions of 60 mm diameter and 20 mm height). A thin perforated copper foil was used on the head of crucible for avoiding powder dispersion in the furnace during thermal decomposition of the precursors.

2.5 *Preparing* of the Modified AP Nanocomposites

To examine the catalytic activity of La_2O_3 and CuO NPs, their nanocomposites with AP were prepared at the first stage. In this order, diverse nanocomposites of AP and different percent of either La_2O_3 or CuO NPs (0.5, 2 and 5 %w/w) were obtained by solvent/ non-solvent technique as suggested

previously [32–34]. Water and MIBK respectively were used as solvent and non-solvent for AP. The AP nanocomposites were obtained by dispersing the accountable mass of NPs in 30.0 mL of MIBK (non-solvent) by ultrasound treatment in an ultrasonic bath for 10 min. At that time, the correlated mass of AP was weighted and hence dissolved in 10.0 mL of distilled water warmed to 80 °C to prepare an AP saturated solution. Thereafter, the AP saturated solution was added drop- by- drop to the MIBK containing dispersed NPs to precipitate AP + NPs nanocomposite. However, all the APs solved in the water was deposited as a composite containing the NPs during few minutes. In the next step, the prepared AP nanocomposites were filtered, then washed three times with 20 mL of the non-solvent (MIBK) and finally dried at room conditions.

3 Results and Discussion

3.1 Fabrication and Characterization of Lanthanum Oxide and Copper Oxide Nanoparticles

Lanthanum oxide and copper oxide NPs were obtained from the calcinations of the carbonate precursors in a furnace at the temperature 650 °C during 3 h under static air atmosphere. The SEM images of the fabricated metal oxide particles are shown in Figure 1. As predicted, the particles of the oxides display a globular morphology. The mean sizes of the lanthanum oxide and copper oxide NPs were determined by their SEM images falling between 35 and 30 nm, respectively. XRD technique was also utilized to characterize the resulted metal oxide NP. As could be seen in Figure 2, both XRD patterns show diffraction peaks with considerable intensities due to the formation of oxide products as pure compounds with high crystallinity. Furthermore, the peaks in Figure 2a are comparable with the crystalline structure of La_2O_3 (JCPDS No 98-011-9010) and the appeared peaks in Figure 2b are in agreement with the XRD spectrum of CuO (JCPDS No. 01-078-0428).

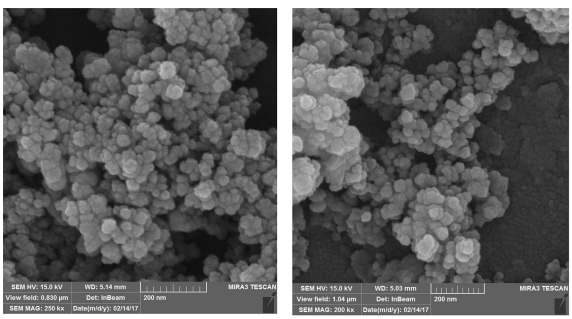

Figure 1. SEM images of the synthesized nano-sized NPs by calcination of their precursors: La_2O_3 (a) and CuO (b).

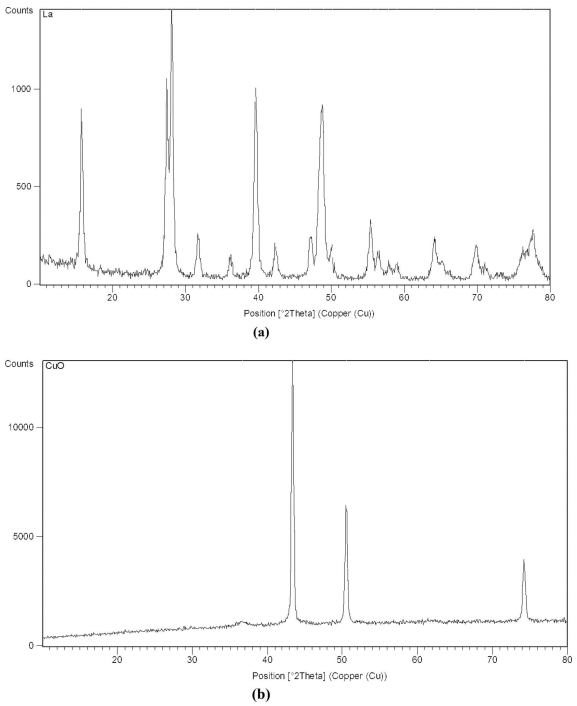

Figure 2. XRD patterns of the synthesized nano-sized NPs by calcination of their precursors: La_2O_3 (a) and CuO (b).

3.2 Characterization of Prepared AP Nanocomposites

The fabricated AP + La_2O_3 and AP + CuO nanocomposites samples containing different percentages of nanocatalysts were examined by SEM to characterize their construction and morphology. Figure 3 displays the resulted SEM images for the nanocomposite samples of AP + La_2O_3 and AP + CuO. The SEM images of AP + La_2O_3 nanocomposites comprising 0.5, 2 and 5 % of La_2O_3 NPs are given in Figure 3a–c, respectively. The images show the same morphologies of the AP particles in all nanocomposite samples, while the AP particles formed as some micrometer-sized units without substantial agglomeration.

AP + CuO nanocomposite samples were also inspected by SEM. The SEM images of the nanocomposite samples comprising 0.5, 2 and 5 % of CuO NPs respectively are given in Figure 3d–f. The images obviously show that CuO NPs are distributed through the AP particles, while AP micrometer-sized particles show no significant agglomeration in all nanocomposite samples.

3.3 Catalytic Activity of La_2O_3 and CuO NPs in AP Nanocomposites

Characterizing thermal behavior of pure AP and its nanocomposites was carried out by TG and DSC techniques. DSC curves of the samples are publicized in Figure 4, while correlated TG thermograms are shown in Figure 5. As can be

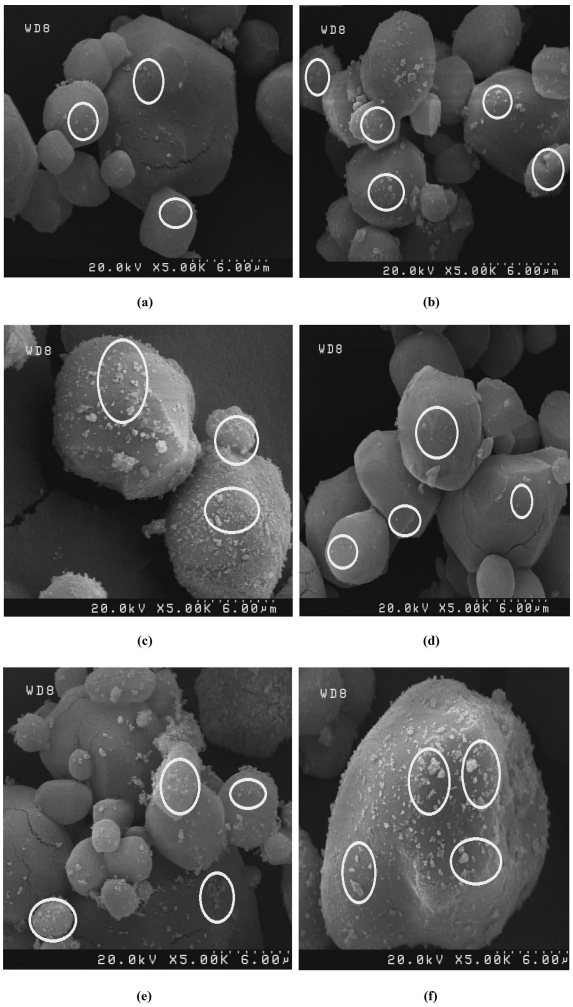

Figure 3. SEM images of AP + La_2O_3 and AP + CuO nanocomposites: (a) AP + 0.5 %La_2O_3; (b) AP + 2 %La_2O_3; (c) AP + 5 %La_2O_3; (d) AP + 0.5 %CuO; (e) AP + 2 %CuO and (f) AP + 5 %CuO.

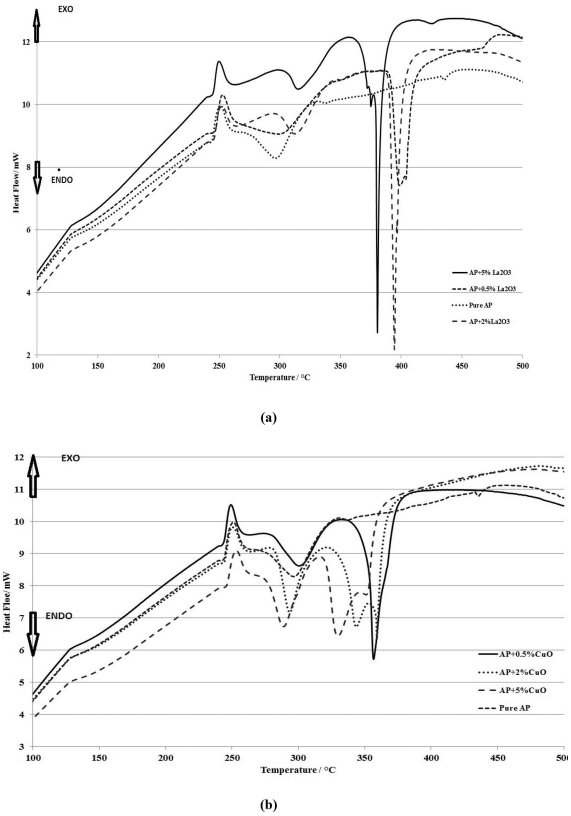

Figure 4. DSC curves of (a) pure AP and AP nanocomposites in the presence of 0.5 % La_2O_3, 2 % La_2O_3 and 5 % La_2O_3 NPs and (b) pure AP and AP nanocomposites in the presence of 0.5 %CuO, 2 %CuO and 5 %CuO NPs. Sample mass 3.0 mg; heating rate 5, 10, 15 and 20 °C.min^{-1} and nitrogen atmosphere.

seen from the DSC curve of pure AP (Figure 4), three consecutive occasions are noticeable throughout the thermal decomposition of this compound. The first reaction appeared at 245.1 °C as an endothermic peak which can be attributed to the phase transition of pure AP from orthorhombic to cubic crystalline form [35]. Two exothermic peaks appeared at higher temperatures. The first one was detected at temperature 289.8 °C. This exothermic event is consistent with the preliminary decomposition of pure AP. The subsequent exothermic event was detected as a peak at the temperature of 421.7 °C, being responsible for decomposition of the preliminary formed intermediates to gaseous products [36]. In the meantime, these decomposition steps described for the pure AP are observable in the TG curve (Figure 5). The pure AP shows two distinct mass losses through its decomposition, as seen in the TG curve. The first shows a 35.3 % decrease in mass and the second happened at a higher temperature with about 64.7 % mass loss. This trend is consistent to earlier reference [37–39].

DSC thermograms of the AP nanocomposites comprising of 0.5, 2 and 5 % La_2O_3NPs are given in Figure 4a. As seen in the figure, La_2O_3 NPs yield surprising catalytic effects on the thermal pattern of AP. In these nanocomposites, the endothermic peak responsible for the phase transition of the AP (approx. 245 °C) displayed some slight shifts (dependent on the catalyst content) to lower temperatures. The thermal decomposition pattern of AP in the presence of La_2O_3 NPs was remarkably varied with respect to pure AP. In fact, DSC curves of the AP samples treated with La_2O_3 NPs (Figure 4a) demonstrate that La_2O_3 NPs enhance the decomposition temperature of the first stage of AP particles. This increment is more pronounced for the sample with higher content of La_2O_3 NPs. On the other hand, these NPs decrease the temperature of the AP decomposition in the second step and again this decrease is dependent on the content of La_2O_3 NPs. Comparing thermal patterns of the AP-La_2O_3 NPs composites with pure AP discloses that addition of 0.5 %, 2 % and 5 % La_2O_3 NPs decreases the temperature of AP second stage of AP decomposition about

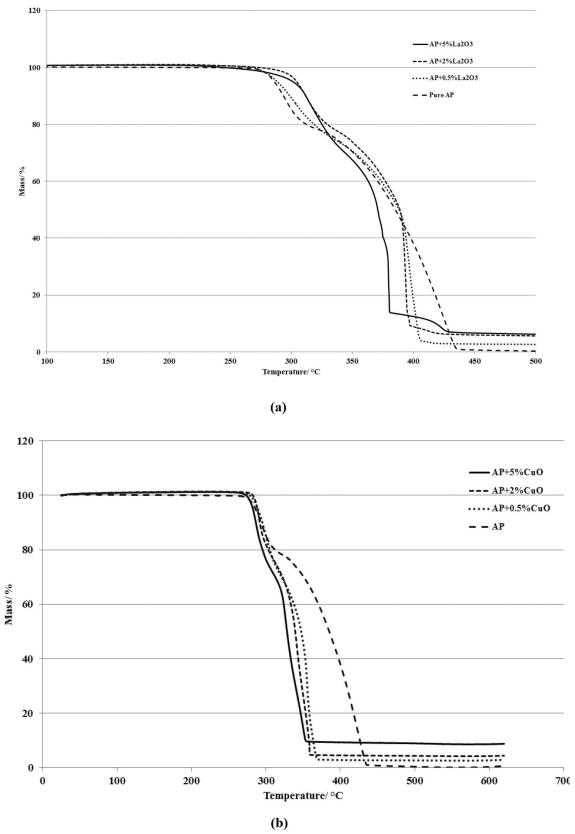

Figure 5. TG curves of (a) pure AP and AP nanocomposites in the presence of 0.5 %La_2O_3, 2 %La_2O_3 and 5 %La_2O_3 NPs and (b) pure AP and AP nanocomposites in the presence of 0.5 %CuO, 2 %CuO and 5 %CuO NPs. Sample mass 3.0 mg; heating rate 10 °min^{-1} and nitrogen atmosphere.

28.3, 30.1 and 71.3 °C, respectively. In fact, introducing La_2O_3 NPs to AP drops the interval temperature of both exothermic stages and supports the merging of both events into single ones (Figure 4a). TG curves of the AP + La_2O_3 NPs nanocomposites are shown in Figure 5a. Adding La_2O_3 NPs to AP particles leads in the final step to a noteworthy decrease of the AP decomposition temperature. Likewise, mass loss attributed to decomposition of AP + La_2O_3 nanocomposites takes places in a single step in contrast to pure AP. Additionally, the heat of decomposition of AP + La_2O_3 nanocomposites is higher than for pure AP. Figure 6 permits comparison of this item for pure AP and AP + La_2O_3 nanocomposite samples. In comparison to pure AP the heat of decomposition was amplified respectively. For pure AP, 0.5 % La_2O_3 + AP, 2 % La_2O_3 + AP and 5 % La_2O_3 + AP were determined 728, 944, 1164 and 1590 J/g.

Thermal patterns of AP + CuO nanocomposites were explored by DSC/TG systems too. The thermograms are represented in the Figure 4b and 5b. These thermograms obviously show the catalytic role of the CuO NPs on the thermal pattern of AP particles. Adding of CuO NPs has no considerable effect on the endothermic peak corresponding

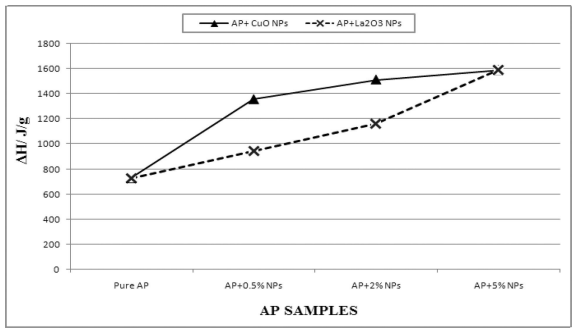

Figure 6. Effect of nanocatalysts (La_2O_3 and CuO) content on the heat of decomposition of AP nanocomposites.

to the phase transition of AP particles. This peak appears at similar temperatures (~245 °C) compared to pure AP. In contrast to pure AP, the temperatures of doublet decomposition stages of AP were remarkably shifted for AP + CuO nanocomposites.

DSC curves of the AP + CuO NPs nanocomposite samples (Figure 4b) confirm the efficient reduction of AP decomposition temperature due to the catalytic activity of CuO NPs. The thermal decomposition temperature of AP at its second step was reduced about 69.8, 66.9 and 104.5 °C in the presence of 0.5 %, 2 % and 5 % CuO NPs compared to the pure AP, respectively. Similar to previous nanocatalyst, CuO NPs improve the thermal behavior of AP particles by reducing the temperature interval between the first and second step of AP decomposition (Figure 4b). Meanwhile, TG curves of pure AP and AP + CuO nanocomposites are shown in Figure 5b. As seen, addition of CuO NPs to AP causes a reduction of AP thermal decomposition temperature at the final stage. AP + CuO nanocomposites decompose and lose their mass during a consecutive step in contrast to pure AP. Besides, CuO NPs addition to AP elevates the heat of decomposition. As seen in Figure 6, addition of 0.5 %, 2 % and 5 % CuO NPs increases the heat of decomposition up to 1356, 1512 and 1588 Jg^{-1} compared to 728 Jg^{-1} for pure AP respectively.

3.4 Comparison of the Catalytic Effect of La_2O_3 to CuO NPs

AP decomposition as a thermally process commonly occurs during three distinct steps including an endothermic and two exothermal events. The endothermic step is due to the orthorhombic phase transferring to the cubic form of AP. This transition occurred at a temperature lower than 250 °C. The exothermal steps happened at higher temperatures due to the AP decomposition spectrum [40]. Two diverse mechanisms have been proposed for the thermal AP decomposition [41–47]. One mechanism includes electron transport from anion to cation (i. e., perchlorate to ammonium), while the other is based on the proton moving from

Table 1. Catalytic activities of La_2O_3 and CuO NPs on temperature and heat of decomposition of ammonium perchlorate.

Sample No	Composition	Thermal temperature/°C			ΔH/J.g^{-1}
		Phase trans.	First event	Second event	
AP0	Pure AP	245.1	289.8	421.7	728
AP1	AP + 0.5 %La_2O_3	243.6	–	393.4	944
AP2	AP + 2 %La_2O_3	241.4	–	391.6	1164
AP3	AP + 5 %La_2O_3	244.3	–	350.4	1590
AP4	AP + 0.5 %CuO	243.6	–	351.9	1356
AP5	AP + 2 %CuO	243.4	–	354.8	1512
AP6	AP + 5 %CuO	242.2	–	317.2	1588

Sample mass 3.0 mg; heating rate 10 °C min^{-1}; N_2 atmosphere.

cation to the anion (i.e., ammonium to perchlorate). Catalytic influence of metal oxides (i.e., La_2O_3 and CuO) on thermal decomposition of this compound is dependent on this electron transfer mechanism in which the metal oxide may acts as a bridge for the electron transport. Accordingly, metal oxides can act as a catalysts and speed up this process [42, 43].

Comparing the thermal behaviors of nanocomposites containing the produced La_2O_3 NPs and CuO NPs by calcination of their precursors provides some attractive results about their catalytic activities. Table 1a bridges the thermal data about influence of nature and percent of NPs on thermal behaviors of the modified AP samples. As seen in the table, the nature and contents of NPs professionally influence the thermal decomposition of the AP samples.

TG data on pure AP illustrate two distinct decomposition stages with about 35.4 % and 64.6 % mass loss during these steps. However, TG data for the samples of AP + La_2O_3 NPs nanocomposite show strong catalytic activity of these NPs for the decomposition of AP particles. Introducing 5 % La_2O_3 NPs to AP composition yields better results than the lower contents with 0.5 and 2 % NPs in reducing AP decomposition temperature in the final stage and giving an upsurge to the decomposition heat. Also, TG data on AP + CuO nanocomposite samples established the key effect of CuO NPs on thermal behavior of AP. Naturally addition of 5 % CuO NP to AP composition has a higher effect on its thermal stability compared to the lower contents. This further effect includes the intensive falling of the AP decomposition temperature at the final stage and a more increment of decomposition heat.

The lower decomposition temperature and higher heat of decomposition in the treated AP samples with the synthesized nanocatalysts could be explained by following elucidations: First, effectual adsorption of the gassy products of the AP decomposition by La_2O_3 and CuO NPs, which encourage the gaseous reaction accordingly [47]. Second, popping of the AP particles during their thermal decomposition is less due to the superior surface area of NPs (high surface area with respect to their volumes). Accordingly, the nanocomposites have less mechanical strength and surface energy, whereas their heat transfer is carried out more efficiently [47]. Finally, the combustion of intermediates (i.e., NH_3 and chlorine oxides) is catalytically speeding up in the presence of the NPs [44].

3.5 Thermo Kinetics of the Nanocomposites Decomposition

Up to date, diverse methods have been established for determination of the kinetic parameters of the decomposition using thermal analysis results [48–50]. In this work, two well-known methods were used to process the DSC results of the nanocomposite samples (Table 2) and therefore computing the Arrhenius parameters (i.e., the activation energy (E_a) and the frequency factor (A) corresponding to the thermal decomposition of AP nanocomposites (AP + 5 % La_2O_3 and AP + 5 % CuO). These samples were examined by DSC under diverse heating rates as AP nanocomposites with optimal decomposition pattern. Kissinger method was the first utilized method in this study [51, 52]:

Table 2. The effect of heating rate on the maximum temperature (T_m) of decomposition of pure AP, **AP + 5 %**La_2O_3 andAP + 5 %CuO nanocomposites.

Heating rate (β)/ °C min^{-1}	Pure AP/ °C	AP + 5 %La_2O_3/ °C	AP + 5 %CuO/ °C
5	413.1	341.1	307.4
10	421.7	350.4	317.2
15	427.9	355	325.2
20	432.1	358.7	328

$$\ln\frac{\beta}{T_m^2} = \ln\frac{AR}{E} - \frac{E}{RT_m} \quad (1)$$

In this formula, β, T_m, and R respectively represent the DSC heating rate, maximum peak temperature and the universal gas constant. In the Kissinger methodology, plotting of ln ($\beta.T_m^{-2}$) against $1/T_m$ is carried out to obtain the activa-

Table 3. Comparison of kinetic parameters for decomposition reaction of pure and nanocomposites of ammonium perchlorate particles (**AP + 5 %CuO and AP + 5 %La_2O_3**).

Samples	**Pure AP**		**AP + 5 %La_2O_3**		AP + 5 %CuO	
Parameter	Kissinger	Starink	Kissinger	Starink	Kissinger	Starink
E_a/kJ mol^{-1}	280.3	280.6	244.1	244.3	178.9	179.2
log A	16.2	16.4	15.6	15.8	10.8	11.1
$\Delta G^{\neq}$/kJ mol^{-1}	240.5	237.2	214.9	212	204.8	202.1
$\Delta H^{\neq}$/kJ mol^{-1}	274.6	274.8	238.9	239.1	174	174.2
$\Delta S^{\neq}$/J mol^{-1} K^{-1}	49.1	54.1	38.5	43.5	−52.1	−47.2
r	0.9969	0.9969	0.9965	0.9965	0.9977	0.9977

tion energy of the decomposition reaction from the slope of the resulted line. Starink method was another utilized methodology in this work for computing the Arrhenius parameters of the AP nanocomposites [52, 53]:

$$\ln(\beta/T_m^{1.92}) + 1.0008E_a/RT_m = C \quad (2)$$

The values of T_m or maximum peak temperatures for all examined samples at dissimilar heating rates (β) of the DSC technique are abridged depicted in Table 2. These results were utilized as input for calculating the activation energy (Ea) of AP nanocomposites by the Kissinger and Starink approaches. Plotting of ln (βT_m^{-2}) against $1/T_m$ (in Kissinger approach) produces straight lines for the pure AP (r = 0.9969), AP + 5 % La_2O_3 (r = 0.9965) and AP + 5 % CuO (r = 0.9977) (see Table 3). These results specify that the mechanism of thermal decomposition of pure AP and nanocomposite samples is constant at the tested temperature range. The slopes of these obtained lines are equal to $-E_a/R$ and hence, the values of activation energy (E_a) were obtained for the different samples. Table 3 comprises calculated values of the activation energy for pure AP and AP + 5 % La_2O_3 and AP + 5 % CuO nanocomposites by Kissinger method. To calculate the activation energy (E_a) for the nanocomposites samples by Starink approach [52, 53], *In* ($\beta/T_m^{1.92}$) was plotted against the inverse of the maximum peak temperature. The results were straight lines for the pure AP (r = 0.9969), AP + 5 % La_2O_3 (r = 0.9965) and AP + 5 % CuO (r = 0.9977).The values of activation energy (E_a) for the different samples were obtained from these slopes and the results are given in Table 3.

Afterwards, the frequency factor (A) for the tested samples was computed by the following formula planned by ASTM E698 [54]:

$$A = \beta\left(\frac{E_a}{RT_m^2}\right) \exp\left(\frac{E_a}{RT_m}\right) \quad (3)$$

The values of log (A) were computed using equation (3) and the results are given in Table 3. By comparing the kinetic parameters obtained for the samples via the applied methods, it could be established that both approaches parade similar trend by yielding comparable values for the activation energies of identical samples. Meanwhile, thermodynamic factors related to the activation of decomposition reaction were attained by the use of the equations (4–6) [55–58]:

$$A \exp\frac{-E}{RT} = \nu \exp\frac{-\Delta G^{\neq}}{RT} \quad (4)$$

$$\Delta H^{\neq} = E - RT \quad (5)$$

$$\Delta G^{\neq} = \Delta H^{\neq} - T\Delta S^{\neq} \quad (6)$$

In these formulae $\Delta G^{\#}$, $\Delta S^{\#}$ and $\Delta H^{\#}$ respectively symbolize the Gibbs free energy, the entropy and the enthalpy of the activation. Additionally, $\upsilon = K_B T/h$ (wherever K_B and h signify the Boltzmann and the Plank constants, respectively). Table 3 represents the calculated values of the kinetic and the thermodynamic factors accountable for pure AP, AP + 5 % La_2O_3 and AP + 5 % CuO nanocomposites. The results demonstrate that adding La_2O_3 or CuO NPs to AP leads to an extensive discount in the values of activation energy (E_a), $\Delta H^{\#}$ and $\Delta S^{\#}$ corresponding to the thermal decomposition of the AP samples. As well, addition of 5 % La_2O_3 or 5 % CuO NPs to AP decreases the values of E_a to 244.1 and 178.9 kJ mol^{-1} respectively, which is roughly 85 % and 65 % of the factor for pure AP (280.3 kJ mol^{-1}). In Table 3, a similar trend could be observed for other activation factors in the nanocomposite samples with respect to pure AP.

4 Conclusion

La_2O_3 and CuO NPs were successfully prepared by calcination of their precursors in the form of carbonate salts. The fabricated NPs were characterized by XRD and SEM methods to analyze their structure and morphology. Their results documented formation of La_2O_3 and CuO as globular NPs, while they possess average particle sizes of approximately 35 and 30 nm, respectively. The fabricated NPs were applied as nanocatalysts in AP compositions, while their catalytic behavior was tested by TG and DSC methods. Thermal analysis results were surprising and demonstrated strong catalytic effects of NPs by substantial drop in the temperature of AP decomposition and augmentation of the heat of decomposition for AP. In addition, the results of the present

study disclosed that E_a, $\Delta H^{\neq}$ and $\Delta S^{\neq}$ of AP in the presence of La_2O_3 and CuO NPs are prominently lower than for the pure AP.

Funding

This research did not receive any specific grant from funding agencies in the public, Commercial, or not-for-profit sectors.

Acknowledgements

We acknowledge Semnan University for its supports.

References

[1] D. R. Paul, L. M. Robeson, Polymer Nanotechnology, Nanocomposites, *Polymer* **2008**, *49*, 3187

[2] Y. Bayat, S. M. Pourmortazavi, H. Iravani, H. Ahadi, Statistical optimization of supercritical carbon dioxide anti solvent process for preparation of HMX nano particles, *J. Supercrit. Fluids* **2012**, *72*, 248.

[3] A. P. Kumar, D. Depan, N. S. Tomer, R. P. Singh, Nano-scale Particles for Polymer Degradation and Stabilization-Trends and Future Perspectives, *Prog. Polym. Sci.* **2009**, *34*, 479.

[4] S. M. Pourmortazavi, S. S. Hajimirsadeghi, M. Rahimi-Nasrabadi, I. Kohsari, Electrosynthesis and characterization of copper oxalate nano particles, *Synth. React. Inorg. Met.-Org. Nano-Met. Chem.* **2012**, *42*, 746.

[5] C. Mahender, B. Murali, V. Himabindu, Synthesis of Nano Phase Titanium Dioxide (TiO_2) in Diffusion Flame Reactor and its Application in Photo-catalytic Reaction, *Int. J. Engine Res.* **2014**, *4*, 209.

[6] M. Rahimi-Nasrabadi, S. M. Pourmortazavi, M. R. Ganjali, S. S. Hajimirsadeghi, M. M. Zahedi, Electrosynthesis and characterization of zinc tungstate nano particles, *J. Mol. Struct.* **2013**, *1047*, 31.

[7] M. Shahidzadeh, P. Shabihi, S. M. Pourmortazavi, Sonochemical preparation of copper(II) chromite nano-catalysts and particle size optimization via Taguchi method, *J. Inorg. Organomet. Polym.* **2015**, *25*, 986.

[8] M. P. Rosynek, Catalytic Properties of Rare Earth Oxides, *Catal. Rev.* **2007**, *16/1*, 111

[9] B. Balusamy, Y. G. Kandhasamy, A. Senthamizhan, G. Chandrasekaran, M. S. Subramanian, K. Tirukalikundram, Characterization and bacterial toxicity of lanthanum oxide bulk and nano particles, *J. Rare Earths* **2012**, *30*, 1298.

[10] M. Rahimi-Nasrabadi, S. M. Pourmortazavi, M. Aghazadeh, M. R. Ganjali, M. Sadeghpour Karimi, P. Norouzi, Synthesis of nanostructured lanthanum tungstates photo-catalysts, *J. Mater. Sci. Mater. Electron.* **2017**, *28*, 7600.

[11] M. Taran, M. Rad, M. Alavi, Antibacterial activity of copper oxide (CuO) nano particles bio synthesized by bacillus sp. FU4, optimization of experiment design, *J. Pharm. Sci.* **2017**, *23*, 198.

[12] J. Zhao, Z. Wang, Y. Dai, B. Xing, Mitigation of CuO nano particle-induced bacterial membrane damage by dissolved organic matter, *J. Water Res.* **2013**, *47*, 4169.

[13] O. Bondarenko, K. Juganson, A. Ivask, K. Kasemets, M. Mortimer, A. Kahru, Toxicity of Ag, CuO and ZnO nano particles to selected environmentally relevant test organisms and mammalian cells in vitro, a critical review, *Arch. Toxicol.* **2013**, *87*, 1181.

[14] Y. W. Hsu, T. K. Hsu, C. L. Sun, Y. T. Nien, N. W. Pu, M. Der Ger, Synthesis of CuO/graphene nanocomposites for nonenzymatic electrochemical glucose biosensor applications, *Electrochim. Acta* **2012**, *82*, 152.

[15] C. Wu, K. Sullivan, S. Chowdhury, G. Jian, L. Zhou, M. R. Zachariah, Encapsulation of perchlorate salts within metal oxides for application as nano-energetic oxidizers, *Adv. Funct. Mater.* **2012**, *22*, 78.

[16] L.-J. Chen, G.-S. Li, P. Qi, L.-P. Li, Thermal decomposition of ammonium perchlorate activated via addition of NiO nano-crystals, *J. Therm. Anal. Calorim.*, **2008**, *92*, 765.

[17] K. Fujimura, A. Miyake, The effect of specific surface area of TiO_2 on the thermal decomposition of ammonium perchlorate, *J. Therm. Anal. Calorim.* **2010**, *99*, 27.

[18] R. P. Prajakta, V. N. Krishnamurthy, S. J. Satyawati, Effect of nano-copper oxide and copper chromite on the thermal decomposition of ammonium perchlorate, *Propellants Explos. Pyrotech.* **2008**, *33*, 266.

[19] L. Chen, L. Li, G. Li, Synthesis of CuO nano-rods and their catalytic activity in the thermal decomposition of ammonium perchlorate, *J. Alloys Compd.* **2008**, *464*, 532.

[20] Z. Yu, L. Chen, L. Lu, X. Yang, X. Wang, DSC/TG-MS study on in situ catalytic thermal decomposition of ammonium perchlorate over CoC_2O_4, *Chin. J. Catal.* **2009**, *30*, 19.

[21] L.-J. Chen, G.-S. Li, L.-P. Li, CuO nano-crystals in thermal decomposition of ammonium perchlorate stabilization, structural characterization and catalytic activities, *J. Therm. Anal. Calorim.* **2008**, *2*, 581.

[22] H. Momenizadeh-Pandas, M. Fazli, Fabrication of MgO and ZnO nano particles by the aid of eggshell bioactive membrane and exploring their catalytic activities on thermal decomposition of ammonium perchlorate, *J. Therm. Anal. Calorim.* **2018**, *131*, 2913.

[23] C. Hu, H. Liu, W. Dong, Y. Zhang, G. Bao, C. Lao, L. Wang Zhong, $La(OH)_3$ and La_2O_3 nanobelts synthesis and physical properties, *J. Adv. Mater.* **2007**, *19*, 470.

[24] B. Tang, J. Ge, C. Wu, L. Zhuo, J. Niu, Z. Chen, Z. Shi, Y. Dong, Sol-solvothermal synthesis and microwave evolution of $La(OH)_3$ nano-rods to La_2O_3 nano-rods, *J. Nanotechnology* **2004**, *15*, 1273.

[25] M. Rahimi-Nasrabadi, S. M. Pourmortazavi, A. A. Davoudi-Dehaghani, S. S. Hajimirsadeghi, M. M. Zahedi, Synthesis and characterization of copper oxalate and copper oxide nano particles by statistically optimized controlled precipitation and calcination of precursor, *CrystEngComm* **2013**, *15*, 4077.

[26] W. M. Abdel-Wareth, X. Xu, Ammonium perchlorate decomposition characteristic parameters determination, a simplified approach, *Appl. Mech. Mater.* **2012**, *110–116*, 155.

[27] J. Liu, Q. Wu, Y. Ding, Y. Yi, Assembling synthesis of barium chromate nano-superstructures using eggshell membrane as template, *Bull. Korean Chem. Soc.***2004**, *25*, 1775.

[28] Q. Dong, H. Sun, J. Xu, D. Zhang, R. Wang, Synthesis of biomorphic ZnO interwoven microfibers using eggshell membrane as the bio-template, *Mater. Lett.*, **2007**, *61*, 2714.

[29] K. Raha, S. Ramamurtly, D. G. Patil, The catalytic effect of rare earth oxidation on the thermal decomposition of AP, *J. Therm. Anal.* **1989**, *35*, 1205.

[30] E. Ayoman, S. G. Hosseini, Synthesis of CuO nano-powders by high-energy ball-milling method and investigation of their cat-

alytic activity on thermal decomposition of ammonium perchlorate particles, *J. Therm. Anal. Calorim.* **2016**, *123*, 1213.
[31] M. Shamsipur, S. M. Pourmortazavi, S. S. Hajimirsadeghi, M. Roushani, Applying Taguchi robust design to the optimization of synthesis of barium carbonate nano-rods via direct precipitation, *Colloids Surf. A* **2013**, *423*, 35.
[32] S. G. Hosseini, S. J. Hosseini-Toloti, K. Babaei, A. Ghavi, The effect of average particle size of nano-Co_3O_4 on the catalytic thermal decomposition of ammonium perchlorate particles, *J. Therm. Anal. Calorim.* **2016**, *124*, 1243.
[33] S. M. Pourmortazavi, M. Rahimi-Nasrabadi, H. Rai, A. Besharati-Seidani, A. Javidan, Role of metal oxide nano-materials on thermal stability of 1, 3, 6-trinitrocarbazole, *Propellants Explos. Pyrotech.* **2016**, *41*, 912.
[34] S. M. Pourmortazavi, M. Rahimi-Nasrabadi, H. Rai, Y. Jabbarzadeh, A. Javidan, Effect of Nano-materials on Thermal Stability of 1, 3, 6, 8-Tetranitro Carbazole, *Cent. Eur. J. Energ. Mater.* **2017**, *14*, 201.
[35] S. G. Hosseini, R. Abazari, A. Gavi, Pure $CuCr_2O_4$ nano particles, Synthesis, characterization and their morphological and size effects on the catalytic thermal decomposition of ammonium perchlorate, *Solid State Sci.* **2014**, *37*, 72.
[36] W. J. Zhang, P. Li, H. B. Xu, R. Sun, P. Qing, Y. Zhang, Thermal decomposition of ammonium perchlorate in the presence of $Al(OH)_3 \cdot Cr(OH)_3$ nano particles, *J. Hazard. Mater.* **2014**, *268*, 273.
[37] M. Rajić, M. Sućeska, Study of Thermal decomposition kinetics of low-temperature reaction of ammonium perchlorate by isothermal TG, *J. Therm. Anal. Calorim.* **2000**, *63*, 375.
[38] J. Zhi, W. Tian-Fang, L. Shu-Fen, Z. Feng-Qi, L. Zi–Ru, Y. Cui-Mei, L. Yang, L. Shang-When, Z. Gang-Zhui, Thermal behavior of ammonium perchlorate and metal powders of different grades, *J. Therm. Anal. Calorim.*, **2006**, *85*, 315.
[39] E. Alizadeh-Gheshlaghi, B. Shaabani, A. Khodayari, Y. Azizian-Kalandaragh, R. Rahimi, Investigation of the catalytic activity of nano-sized CuO, Co_3O_4 and $CuCo_2O_4$ powders on thermal decomposition of ammonium perchlorate, *Powder Technol.*, **2011**, *217*, 330.
[40] J. Wang, S. He, Z. Li, X. Jing, M. Zhang, Z. Jiang, Self-assembled CuO nano-architectures and their catalytic activity in the thermal decomposition of ammonium perchlorate, *J. Colloid. Polym. Sci.* **2009**, *287*, 853.
[41] B. L. Dubey, N. B. Singh, J. N. Srivastava, A. K. Ojha, The catalytic behavior of $NiFe_{2-x}Cr_xO_4$ ($0.0 \leq x \leq 2.0$) during the thermal decomposition of ammonium perchlorate, polystyrene and their composite propellants, *Indian J. Chem.* **2001**, *40 A*, 841.
[42] E. S. Freeman, D. A. Anderson, Effects of radiation and doping on the catalytic activity of magnesium oxide on the thermal decomposition of potassium perchlorate, *Nature* **1965**, *206*, 378.
[43] C. Li, Y. Yin, H. Hou, N. Fan, F. Yuan, Y. Shi, Q. Meng, Preparation and characterization of $Cu(OH)_2$ and CuO nano-wires by the coupling route of micro-emulsion with homogenous precipitation, *Solid State Commun.***2010**, *150*, 585.
[44] S. S. Joshi, P. R. Patil, V. N. Krishnamurthy, Thermal decomposition of ammonium perchlorate in the presence of nano sized ferric oxide, *Def. Sci. J.* **2008**, *58*, 721.
[45] V. V. Boldyrev, Thermal decomposition of ammonium perchlorate, *Thermochim. Acta* **2006**, *443*, 1.
[46] L. Chen, L. Li, G. Li, Synthesis of CuO nano-rods and their catalytic activity in the thermal decomposition of ammonium perchlorate, *J. Alloys Compd.* **2008**, *464*, 532.
[47] P. R. Patil, V. N. Krishnamurthy, S. S. Joshi, Differential scanning calorimetric study of HTPB based composite propellants in presence of nano ferric oxide, *Propellants Explos. Pyrotech.* **2006**, *31*, 442.
[48] A. Eslami, S. G. Hosseini, V. Asadi, The effect of microencapsulation with nitrocellulose on thermal properties of sodium azide particles, *Prog. Org. Coat.* **2009**, *65*, 269.
[49] A. Eslami, S. G. Hosseini, Improving safety performance of lactose-fueled binary pyrotechnic systems of smoke dyes, *J. Therm. Anal. Calorim.* **2011**, *104*, 671.
[50] A. Eslami, S. G. Hosseini, S. M. Pourmortazavi, Thermo analytical investigation on some boron-fuelled binary pyrotechnic systems, *Fuel* **2008**, *87*, 3339.
[51] H. E. Kissinger, Reaction kinetics in differential thermal analysis, *Anal. Chem.* **1957**, *29*, 1702.
[52] S. Vyazovkin, A. K. Burnham, J. M. Criado, L. A. Pérez-Maqueda, C. Popescu, N. Sbirrazzuoli, ICTAC Kinetics committee recommendations for performing kinetic computations on thermal analysis data, *Thermochim. Acta* **2011**, *520*, 1.
[53] M. J. Starink, The determination of activation energy from linear heating rate experiments, a comparison of the accuracy of isoconversion methods, *Thermochim. Acta* **2003**, *404*, 163.
[54] ASTM E698-05, Standard test method for Arrhenius kinetic constants for thermally unstable materials, doi, 10.1520/E0698-05.
[55] H. Abusaidi, H. R. Ghaieni, S. M. Pourmortazavi, S. H. Motamed-Shariati, Effect of nitro content on thermal stability and decomposition kinetics of nitro-HTPB, *J. Therm. Anal. Calorim.* **2016**, *124*, 935.
[56] J. A. F. F. Rocco, J. E. S. Lima, A. G. Frutuoso, K. Iha, M. Ionashiro, J. R. Matos, M. E. V. Suarez-Iha, TG studies of a composite solid rocket propellant based on HTPB-binder, *J. Therm. Anal. Calorim.* **2004**, *77*, 803.
[57] S. M. Pourmortazavi, M. Rahimi-Nasrabadi, I. Kohsari, S. S. Hajimirsadeghi, Non-isothermal kinetic studies on thermal decomposition of energetic materials, *J. Therm. Anal. Calorim.* **2012**, *110*, 857.
[58] S. M. Pourmortazavi, Kh. Farhadi, V. Mirzajani, S. Mirzajani, I. Kohsari, Study on the catalytic effect of diaminoglyoxime on thermal behaviors, non-isothermal reaction kinetics and burning rate of homogeneous double-base propellant, *J. Therm. Anal. Calorim.* **2016**, *125*, 121.

Received: January 30, 2018
Revised: August 17, 2018
Published online: October 10, 2018

